

Novel infrared-blocking aerogel scattering filters and their applications in astrophysical and planetary science observations

Kyle R Helson^{a,b}, Stefan Arseneau^d, Alyssa Barlis^b, Charles L. Bennett^d, Thomas M. Essinger-Hileman^b, Haiquan Guo^e, Tobias Marriage^d, Manuel A. Quijada^b, Ariel E. Tokarz^d, Stephanie L. Vivod^c, and Edward J. Wollack^b

^aThe University of Maryland, Baltimore County. Baltimore, Maryland, USA

^bNASA Goddard Space Flight Center, Greenbelt, Maryland, USA

^cNASA Glenn Research Center, Cleveland, Ohio, USA

^dThe Johns Hopkins University, Baltimore, Maryland, USA

^eUniversities Space Research Association, Columbia, Maryland, USA

ABSTRACT

Infrared-blocking scattering aerogel filters have a broad range of potential applications in astrophysics and planetary science observations in the far-infrared, sub-millimeter, and microwave regimes. Successful dielectric modeling of aerogel filters allowed the fabrication of samples to meet the mechanical and science instrument requirements for several experiments, including the Sub-millimeter Solar Observation Lunar Volatiles Experiment (SSOLVE), the Cosmology Large Angular Scale Surveyor (CLASS), and the Experiment for Cryogenic Large-Aperture Intensity Mapping (EXCLAIM). Thermal multi-physics simulations of the filters predict their performance when integrated into a cryogenic receiver. Prototype filters have survived cryogenic cycling to 4K with no degradation in mechanical properties.

Keywords: aerogel, infrared, far-IR, sub-millimeter, microwave, metamaterial, filter

1. INTRODUCTION

Cryogenic telescope receivers common in the far-infrared, sub-millimeter, and microwave regimes require strong out-of-band infrared rejection in order to maintain cryogenic performance. A variety of different strategies have been employed to realize thermal blocking structures, which include reflective meshes, absorptive, and scattering designs.¹⁻⁹ These low-pass filters have been implemented using a variety of different materials.

We report on the continued development of broadband, tunable, polymer aerogel-based infrared-blocking filters for millimeter, sub-millimeter, and far infrared observations in planetary science and astrophysics, first reported in Ref. 10. The filters presented are primarily polyimide aerogels¹¹⁻¹³ loaded with diamond scattering particles ranging from 1 to 60 microns, although different polymers for the host aerogel matrix have been explored. These filters have strong out-of-band rejection but also a low index of refraction, ($n \simeq 1.15$) eliminating the need for anti-reflection (AR) coating. These filters function primarily by scattering away unwanted light and subsequently preventing it from reaching the coldest parts of the receiver.

2. OPTICAL MODELING AND FILTER DESIGN

Filter optical design relies primarily on a Mie scattering dielectric model.¹⁰ Mie scattering occurs because of the contrast between the higher index of refraction of the embedded particles and the lower index of the surrounding medium. Table 1 shows a summary of material and optical properties of substrates used to construct aerogel scattering filters. While this publication focuses only on diamond-loaded polyimide aerogels, data for silica and

Further author information: (Send correspondence to Kyle Helson.)

Kyle Helson: E-mail: kyle.helson@nasa.gov

silicon are provided for context. Even though bulk polyimide has an index of refraction of 1.7, due to the low volume filling fraction of an aerogel, an unloaded polyimide aerogel typically has an index of refraction of about 1.1. The diamond-loaded aerogel filters have an index of refraction typically less than 1.2.

Material	Index of Refraction, n	Density [$\frac{g}{cc}$]
Silica	1.95	2.65
Polyimide	1.7	1.42
Silicon	3.4	2.33
Diamond	2.38	3.53

Table 1. Materials properties for bulk components of scattering aerogel filters. Early prototypes used a variety of materials, but the filters in this publication used only polyimide and diamond.

Early filter prototypes from Ref. 10 were fabricated with silicon powder produced by grinding up float-zone silicon wafers in a ball mill. The resulting powder was sieved through meshes of various sizes, down to US 140 mesh size, or 106 microns. This produced a powder that had a broad, non-uniform particle size distribution. Early modeling efforts assumed this to be a uniform size distribution in particle radius, however later analysis showed a significant excess of smaller particles. The large dispersion in the particle size distribution produced by ball milling and subsequent sieving process is responsible for the relatively soft cut-off frequency in the measurement and the disagreement between measurement and model seen in the left plot of Figure 1.

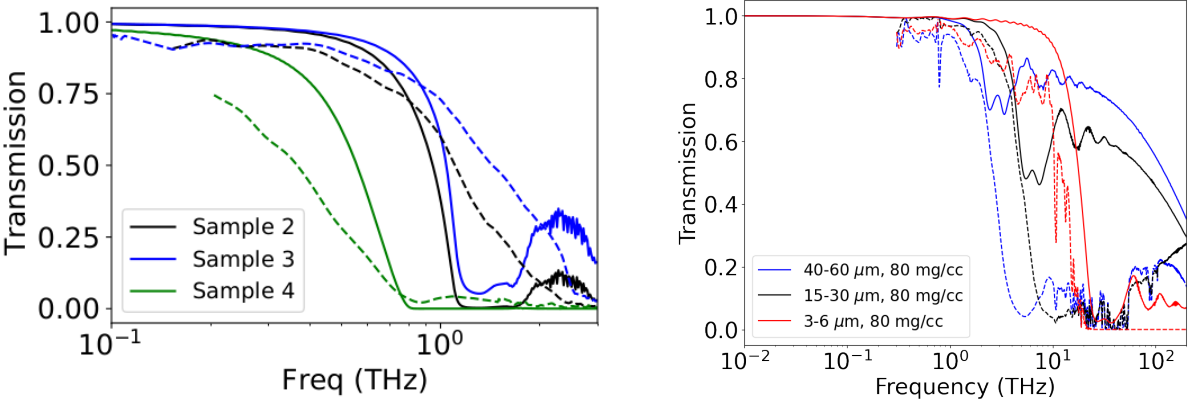


Figure 1. Comparison between early model versus measurement and current modeling versus measurement. *Left*: Comparison of Mie scattering model and measured silica aerogels with silicon particles. Solid lines represent the aerogel dielectric model, while the dashed lines are measured transmission spectra. *Right*: Comparison three different diamond-loaded polyimide aerogel sample transmission data (dashed lines) and their respective Mie scattering models (solid lines). Transmission data and model are scaled to represent 200 μm thick films loaded at 80 mg/cc. Blue curves are for a filter with 40-60 μm particles, black curves are for a filter with 15-30 μm particles, and the red curves are for a filter with 3-6 μm particles. While the very high frequency disagreement still persists, especially for larger particles, the current Mie scattering model predicts filter cutoff frequencies better than the early model.

Figure 1 shows a comparison of transmission spectra between earlier modeling and fabrication efforts and more recent ones. Ultimately commercial, off-the-shelf industrial diamond particles were chosen as scattering media. We selected powders of 1-3, 3-6, 6-12, 10-20, 15-30, 20-40, and 40-60 micron distributions. All powders are from the PUREON Microdiamant MONO-ECO monocrystalline synthetic diamond. Per the manufacturer, particle size distributions are approximately Gaussian, with the end ranges representing the approximate three standard deviation limits for particle diameter. Table 2 shows a sub-sample of particle size distribution data. The particle size distributions are much more tightly controlled than the silicon powder made in-house. Diamond powder composition, particle sizes and shapes were later analyzed with optical microscopy, particle size analysis, and Raman spectroscopy. Figure 2 shows images of the diamond particles and the silicon particles.

The diamond particle size and loading density is controlled to tune the filter to the desired cutoff frequency.

Powder Size Range	Median Size
3-6 μm	4.2 μm
6-12 μm	9 μm
15-30 μm	22.5 μm
40-60 μm	47 μm

Table 2. Diamond particle size distributions and median sizes. All diamond powders are from the PUREON Microdiamant MONO-ECO monocrystalline synthetic diamond. Median particle sizes all fall well within the stated specifications from the manufacturer.

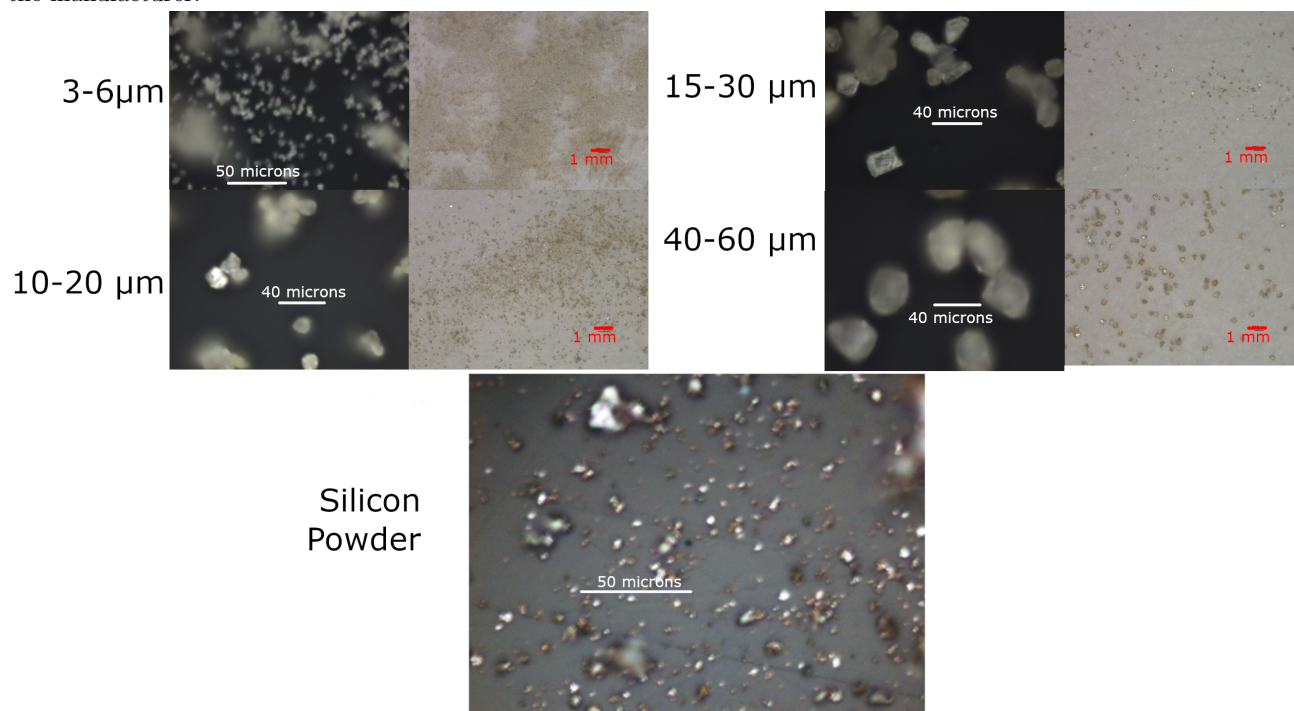


Figure 2. Optical microscope images of some of the diamond and silicon powder samples. *Top*: Diamond size ranges represent the approximate three standard deviation size points, per the manufacturer. *Bottom*: Even after sieving, in-house made silicon powder contained a wide size distribution with many smaller particles.

Particle size has the strongest effect on cutoff frequency. Larger particles have a lower cut-off frequency and smaller particles have a higher cut-off frequency. Polyimide aerogel filters have been fabricated with a range of scatterer loading densities ranging from 20 mg/cc up to 100 mg/cc. For a given particle size distribution, increasing the loading density creates a filter with a lower cut-off frequency and vice versa. For a given loading density, smaller particles produce a stronger cutoff than larger particles because scattering cross-section goes as the square of the particle radius ($\text{area} \propto r^2$) and mass density goes as the cube of particle radius ($\text{volume} \propto r^3$). Figure 3 shows the effects of varying particle radius and density on the predicted filter cutoff frequency. Multiple particle size distributions and densities can be mixed together, e.g. primarily using a higher density of larger particles to set the primary cut-off frequency and mixing in lower densities of smaller particles to control high frequency leakage.

Since first reported, continued development of the Mie scattering model has yielded additional features that allow us to capture the behavior of multiple size distributions of particles as well as include the absorption and emission features of the base polymer chemistry in the transmission curve predictions. A more detailed discussion is presented in Section 3. Additionally, the tightly constrained diamond particle size distributions bring the predicted filter behavior in more agreement with the measured data than in Ref 10. See Ref 14, for details regarding the optical measurements of film samples. Mie scattering modeling code is now also able to accommodate user defined particle size distributions, beyond basic uniform and Gaussian options.

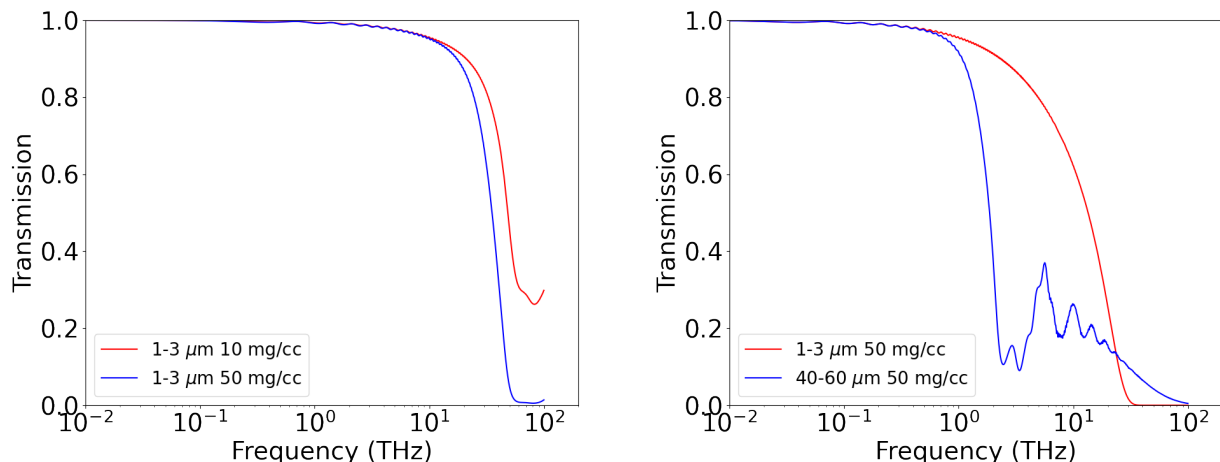


Figure 3. Demonstration of the effect of scattering particle loading density and radius on filter cut-off frequency. *Left:* Comparison of Mie scattering model for different loading densities of the same particle size distribution. Both curves show the transmission of a 0.2 mm thick filter filter with 1-3 μm diamond particles but the red curve is for 10 mg/cc density and the blue curve is for 50 mg/cc. *Right:* Comparison of Mie scattering model for equal loading densities of different particle size distributions. Both curves show the transmission of a 2 mm thick filter filter with 50 mg/cc of diamond particles but the red curve is for 1-3 μm and the blue curve is for 40-60 μm .

2.1 Designing Filters for Specific Missions

With a greater control of filter cut-off frequencies, in-band transmission, and knowledge of the base aerogel transmission spectrum, it is possible to design filters to meet specific mission requirements. During the development and prototyping of filters, filters for three different missions were designed, fabricated, and characterized.

The first experiment is the Sub-milliter Solar Observation Lunar Volatiles Experiment (SSOLVE), which will observe lines from HDO, H₂O, and OH molecules in the lunar atmosphere at 23 GHz, 500 GHz, and 2.5 THz, respectively.¹⁵ SSOLVE requires good rejection of higher frequency THz light but greater than 90% transmission at 2.5 THz. Figure 4 shows a comparison of different diamond-loaded polyimide aerogel designed to meet the SSOLVE requirements.

Filters have also been designed and fabricated to meet the needs of experiments that observe in the microwave regime, like the Cosmology Large Angular Scale Surveyor (CLASS), a cosmic microwave background (CMB) polarimeter designed to observe from the ground from 33-234 GHz.¹⁶ Filters designed for use in microwave observations are also being prototyped for the upcoming Experiment for Cryogenic Large-Aperture Intensity Mapping (EXCLAIM), which is a balloon-borne spectrometer that will carry out a line intensity mapping survey at frequencies from 420-540 GHz, targeting carbon monoxide and ionized carbon emissions from galaxies in redshift slices covering $z = 0 - 3.5$.¹⁷ Figure 4 shows several different prototype filters for these two missions.

3. EXPLORING AEROGEL POLYMER CHEMISTRIES

Scattering aerogel filters have been manufactured with silica and polyimide base aerogels, as well as with silicon and diamond scattering particles.¹⁰ As demonstrated in Ref. 12, polyimide aerogels synthesized with different diamines produce backbone structures with varying mechanical properties. However, different backbone structures may also vary the in-band transmission for infrared blocking applications. Initially, two formulations were identified for further investigation:

- 4,4'-Bis (4-aminophenoxy) biphenyl (BAPB) (25mol%); with 2,2'-Dimethylbenzidine (DMBZ)(75mol%); 3,3',4,4'-biphenyltetracarboxylic dianhydride (BPDA); and 1,3,5- triaminophenoxybenzene (TAB), aka the "BAPB-based polyimide"

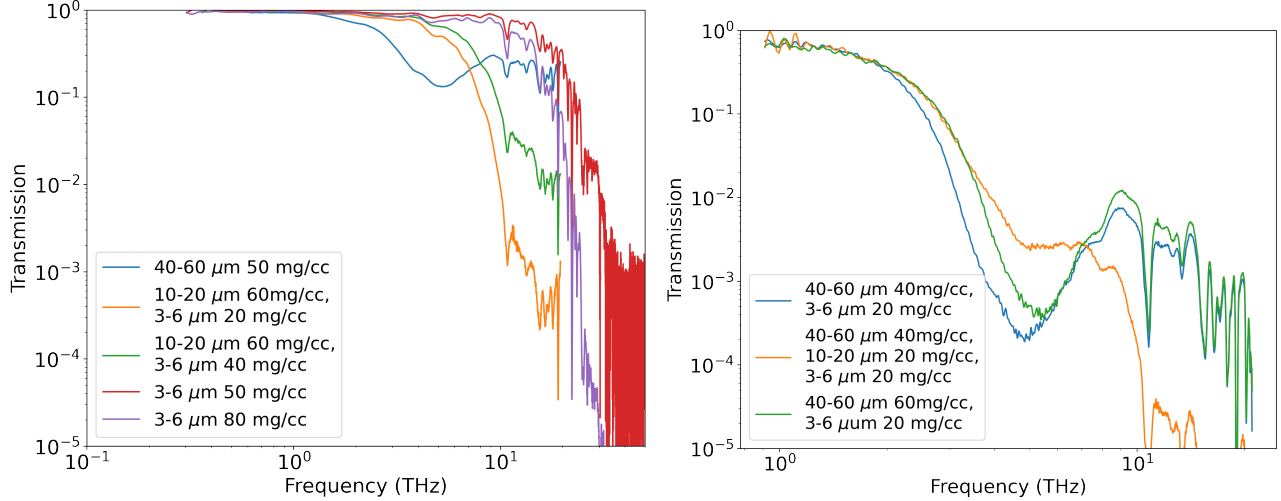


Figure 4. *Left*: Transmission data for four different diamond-loaded polyimide aerogel filters for the SSOLVE mission. Because not all of the prototype filters are the same thickness, all filter transmission data were scaled to represent a 200 μm thick sample. *Right*: Transmission data for three different diamond-loaded polyimide aerogel filters for the CLASS and EXCLAIM missions. Because not all of the prototype filters are the same thickness, all filter transmission data were scaled to represent a 1 mm thick sample. CLASS is a ground-based CMB polarimeter observes the polarized microwave sky from 33-2340 GHz, and EXCLAIM is a balloon-borne spectrometer designed to survey at frequencies from 420-540 GHz.

- 1,12-dodecyl diamine (DADD)(40 mol%); with DMBZ (60 mol%); BPDA; and TAB, aka the “DADD-based polyimide”.

As shown in Figure 5, the two different polymers show similar absorption features around 10-20 THz, however the BAPB formulation shows measurably higher low-frequency transmission, so this formulation was used for the vast majority of the prototype filters.

Measuring the optical performance of the different polyimide backbone formulations also enabled the incorporation of the base aerogel properties into the Mie scattering model. Including the dielectric properties of the base aerogel into the model creates more realistic predictions of filter cutoff frequency as well as in-band transmission. Figure 5 shows a model filter with the DADD-based and BAPB-based polymers incorporated. Other polyimide polymer formulations were also explored, including 7wt% pyrometallic dianhydride (PMDA)+DMBZ/1,3,5-benzenetricarbonyl trichloride (BTC) and 9wt% PMDA+DMBZ/BTC films. Preliminary results suggest the 7wt% PMDA+DMBZ/BTC polyimide formulation to have better in-band transmission than the BAPB-based formula. During the continued development of the polyimide-based aerogels, efforts were made to identify different polymers that might provide better in-band transmission and reduced absorption. Cyclic olefin copolymer (COC) plastics have been identified as promising candidates for aerogel substrates. The COC polymers were chosen for their high in-band transmission and reduced absorption¹⁸ compared to the polyimide formulations. Prototype unloaded and diamond-loaded COC aerogel filters are being manufactured.

4. THERMAL MODELING

The performance of the aerogel filters in a cryogenic receiver will ultimately determine their utility in future missions. Filter equilibrium temperatures and subsequent conductive and radiative thermal loading are key benchmarks. Thermal finite element models of the polyimide aerogel scattering filters were constructed with COMSOL Multiphysics software. The CLASS receiver filter geometry was used as a representative filter implementation. The filter stack consists of three vertically stacked filters over two filter stages, at 60 K and 4 K respectively. The model calculates the background infrared loading on the 4 K stage after loading from a 250 K surface passes through the upper filters. The polyimide aerogel filter performance was compared with model alumina and polytetrafluoroethylene (PTFE) filters. The thermal conductivities of each material are described in Table 3.

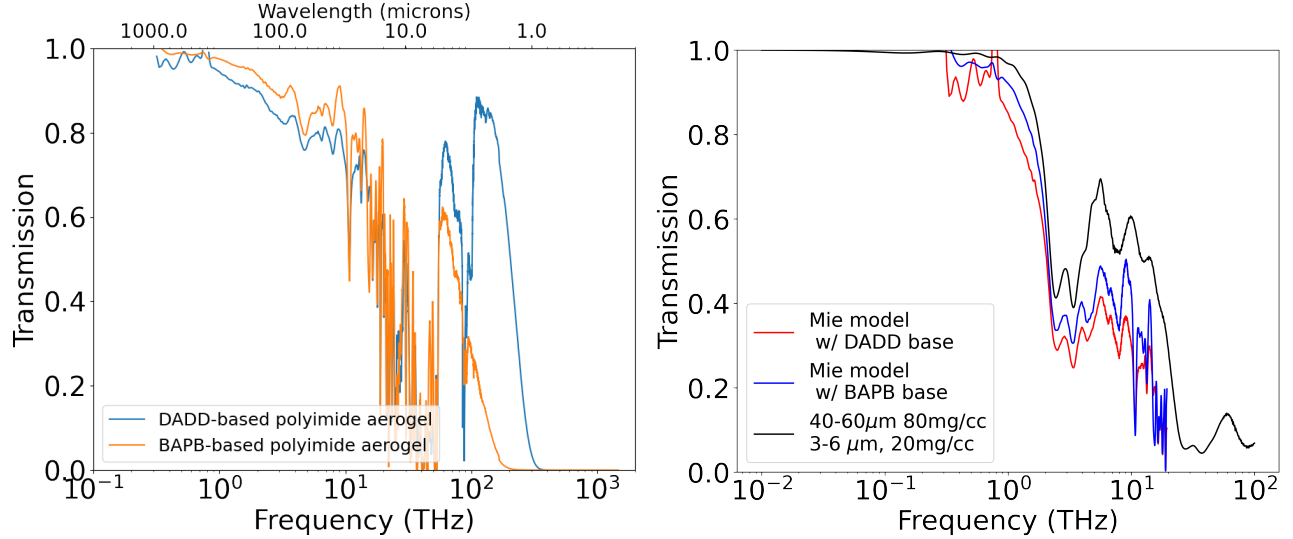


Figure 5. *Left*: Comparison of the transmission spectra of two different unloaded polyimide aerogels. BAPB-based formulation is BAPB(25mol%)+DMBZ (75mol%)/BPDA/TAB, while the DADD-based formulation is DADD(40 mol%)+DMBZ (60mol%)/BPDA/TAB. Transmission spectra are scaled to represent 200 micron thick films. *Right*: Model filter transmission spectra incorporating two different polyimide backbone formulations in order to allow better prediction of cutoff frequency and in-band transmission. The black curve is the Mie model alone, while the red and blue curves are the Mie model incorporating the base aerogel properties. Transmission spectra are for a 0.5 mm thick film.

Material	Thermal Conductivity [$\frac{W}{mK}$]
Diamond-loaded polyimide aerogel	0.024
Alumina	27
PTFE	0.24

Table 3. Summary of material properties used in COMSOL thermal finite element analysis models. Alumina and PTFE are commonly used materials for infrared rejection in cryogenic telescope receivers in the sub-millimeter and microwave.

The first two filters are mounted to the 60 K stage and the side wall of the optics tube around the top two filters is held at 60 K. The third filter was mounted to the 4 K stage and the sidewall along the bottom filter as well as the wall between the last filter and the focal plane were held at 4 K. The surface above the top of the first filter is held at 250 K to simulate the radiation incoming from the stage that sits above the 60 K stage in the CLASS receiver. The separation of filters within the 60K stage of the receiver can be varied to minimize the background radiation that reached the 4 K stage. The geometry of the filters from the COMSOL model is shown in Figure 6.

The COMSOL radiation module was used to estimate the total thermal load on the 4 K stage. In addition to the thermal loading from electromagnetic radiation, the COMSOL model also includes the thermal loading due to conduction through the parts of the filter stack in physical contact with other components of the receiver. The emissivity of the aerogel, alumina, and PTFE filters was swept parametrically from $\epsilon = 0.05$ to 0.9, in order to predict filter performance across a wide range of physical parameters. A total equilibrium thermal load on the third filter was calculated for each emissivity. Figure 7 shows the comparison of the performance between the three different filter substrates. The two 60 K filters are held at the nominal CLASS receiver spacing of 43 mm. A stack of three alumina filters shows the most power rejection by several orders of magnitude. The results are a bit misleading, however, because most implementations of alumina filters do not use a stack of three because of their lower in-band transmission. Alumina filters also have increased cost and more complex AR-coating requirements, due to the high index of refraction, $n \simeq 3.1$. The performance of the aerogel filters depends strongly on the emissivity, but they meet the CLASS thermal loading requirement of less than 100 mW as long as the emissivity is below 0.5. In contrast, alumina and PTFE filters are high emissivity by design, with expected emissivities of 0.75 and 0.97 respectively, set by reflectivity from the surface.

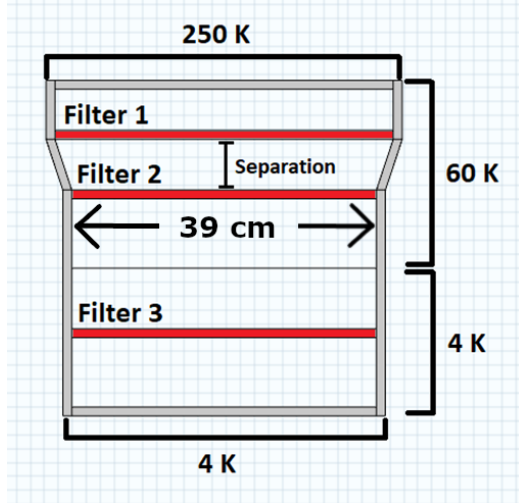


Figure 6. Schematic of the three filter stack inside of the CLASS receiver. The first two filters are both mounted at the 60 K stage but with a variable gap between them. The third filter is mounted to the 4 K stage. The 250 K surface represents the backside of the stage above the 60 K. As pictured, the two 60 K filters are 43 mm apart.

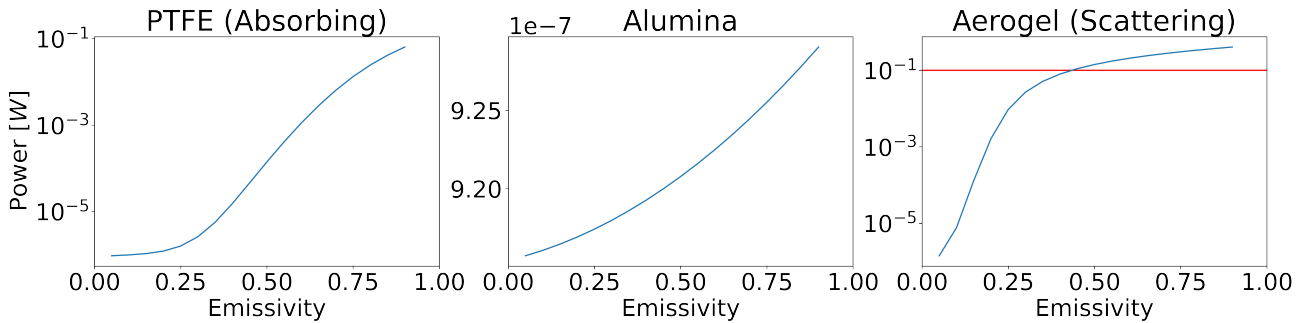


Figure 7. Total thermal load on the third filter for three different filter substrates and a range of emissivity values. The two 60 K filters are spaced 43 mm apart. The left plot is for absorbing PTFE filters, the middle plot for alumina filters, and the right plot is for the diamond loaded polyimide aerogel filters. Three alumina filters provide the greatest rejection of background loading power, but with lower in-band transmission and greater cost and complexity. Additionally, most implementations of alumina filters do not use a three filter stack. The simulation results depend strongly on the emissivity of the aerogel filters. CLASS requires less than 100 mW of load, indicated by the red horizontal line in the right plot.

A second simulation of aerogel filters was run to determine the optimal filter spacing of the 60 K stack. Total thermal load on the 4 K filter was calculated for spacing ranging from 27 mm to 120 mm at emissivities of 0.1, 0.5, and 0.9. The current CLASS design has a spacing of 43 mm. Maximal filter spacing minimizes thermal loading in all cases, by approximately a factor of 5. The data suggest that spacing the 60 K filters as distant apart as is reasonable is optimal. Cryogenic testing to verify the predicted thermal performance of the aerogel scattering filters is expected to begin in the fourth quarter of 2022.

5. CONCLUDING REMARKS

Diamond-loaded polyimide aerogel scattering filters are a promising emerging filter technology for use in far-infrared, sub-millimeter, and microwave astrophysics, cosmology, and planetary science missions. Prototype filters demonstrate excellent out-of-band rejection, high in-band transmission, and tunable cut-off frequencies. Filters are being manufactured in large diameters (larger than 40 cm) and cryogenic testing is underway to verify their performance. In addition to polyimide aerogel filters, other polymeric aerogel filters are being explored and will potentially yield better in-band transmission with reduced in and out-of-band absorption.

ACKNOWLEDGMENTS

The authors would like to thank Aerogel Technologies, LLC, for their assistance in manufacturing film prototypes while NASA facilities were closed due to the COVID-19 pandemic. The material is based upon work supported by NASA under award number 80GSFC21M0002.

REFERENCES

- [1] Ulrich, R., “Far-infrared properties of metallic mesh and its complementary structure,” *Infrared Physics* **7**(1), 37–55 (1967).
- [2] Ulrich, R., “Effective low-pass filters for far infrared frequencies,” *Infrared Physics* **7**(2), 65–74 (1967).
- [3] Ade, P., Pisano, G., Tucker, C., and Weaver, S., “A review of metal mesh filters,” *Proceedings of SPIE - The International Society for Optical Engineering* **6275** (07 2006).
- [4] Bock, J. J. and Lange, A. E., “Performance of a low-pass filter for far-infrared wavelengths,” *Appl. Opt.* **34**, 7254–7257 (Nov 1995).
- [5] Halpern, M., Gush, H. P., Wishnow, E., and Cosmo, V. D., “Far infrared transmission of dielectrics at cryogenic and room temperatures: glass, fluorogold, eccosorb, stycast, and various plastics,” *Appl. Opt.* **25**, 565–570 (Feb 1986).
- [6] Munson, C. D., Choi, S. K., Coughlin, K. P., McMahon, J. J., Miller, K. H., Page, L. A., and Wollack, E. J., “Composite reflective/absorptive ir-blocking filters embedded in metamaterial antireflection-coated silicon,” *Appl. Opt.* **56**, 5349–5354 (Jul 2017).
- [7] Timusk, T. and Richards, P. L., “Near millimeter wave bandpass filters,” *Appl. Opt.* **20**, 1355–1360 (Apr 1981).
- [8] Choi, J., Ishitsuka, H., Mima, S., Oguri, S., Takahashi, K., and Tajima, O., “Radio-transparent multi-layer insulation for radiowave receivers,” *Review of Scientific Instruments* **84**(11), 114502 (2013).
- [9] Whitbourn, L. B. and Compton, R. C., “Equivalent-circuit formulas for metal grid reflectors at a dielectric boundary,” *Appl. Opt.* **24**, 217–220 (Jan 1985).
- [10] Essinger-Hileman, T., Bennett, C. L., Corbett, L., Guo, H., Helson, K., Marriage, T., Meador, M. A. B., Rostem, K., and Wollack, E. J., “Aerogel scattering filters for cosmic microwave background observations,” *Appl. Opt.* **59**, 5439–5446 (Jun 2020).
- [11] Guo, H., Meador, M. A. B., Cashman, J. L., Tresp, D., Dosa, B., Scheiman, D. A., and McCorkle, L. S., “Flexible polyimide aerogels with dodecane links in the backbone structure,” *ACS Applied Materials & Interfaces* **12**(29), 33288–33296 (2020). PMID: 32586090.
- [12] Guo, H., Meador, M. A. B., McCorkle, L., Quade, D. J., Guo, J., Hamilton, B., and Cakmak, M., “Tailoring properties of cross-linked polyimide aerogels for better moisture resistance, flexibility, and strength,” *ACS Applied Materials & Interfaces* **4**(10), 5422–5429 (2012). PMID: 22956659.
- [13] Meador, M. A. B., Malow, E. J., Silva, R., Wright, S., Quade, D., Vivod, S. L., Guo, H., Guo, J., and Cakmak, M., “Mechanically strong, flexible polyimide aerogels cross-linked with aromatic triamine,” *ACS Applied Materials & Interfaces* **4**(2), 536–544 (2012). PMID: 22233638.
- [14] Barlis, A., Arseneau, S., Bennett, C. L., Essinger-Hileman, T., Guo, H., Helson, K. R., Marriage, T., Quijada, M. A., Tokarz, A. E., Vivod, S. L., and Wollack, E. J., “Characterization of aerogel scattering filters for astronomical telescopes,” in [*Millimeter, Submillimeter, and Far-Infrared Detectors and Instrumentation for Astronomy XI*], Zmuidzinas, J. and Gao, J.-R., eds., SPIE (2022).
- [15] Bulcha, B., Anderson, C. M., Chin, G., Shappirio, M., Ehsan, N., Racette, P. E., Hewagama, T., Livengood, T. A., Hesler, J., and Wylde, R., “Submillimeter solar observation lunar volatiles experiment (ssolve) optics and front-end spectrometer,” in [*2021 46th International Conference on Infrared, Millimeter and Terahertz Waves (IRMMW-THz)*], 1–1 (2021).
- [16] Harrington, K., Marriage, T., Ali, A., Appel, J. W., Bennett, C. L., Boone, F., Brewer, M., Chan, M., Chuss, D. T., Colazo, F., Dahal, S., Denis, K., Dünner, R., Eimer, J., Essinger-Hileman, T., Fluxa, P., Halpern, M., Hilton, G., Hinshaw, G. F., Hubmayr, J., Iuliano, J., Karakla, J., McMahon, J., Miller, N. T., Moseley, S. H., Palma, G., Parker, L., Petroff, M., Pradenas, B., Rostem, K., Sagliocca, M., Valle, D., Watts, D., Wollack, E., Xu, Z., and Zeng, L., “The Cosmology Large Angular Scale Surveyor,” in [*Millimeter, Submillimeter,*

and Far-Infrared Detectors and Instrumentation for Astronomy VIII], Holland, W. S. and Zmuidzinas, J., eds., **9914**, 380 – 400, International Society for Optics and Photonics, SPIE (2016).

- [17] Essinger-Hileman, T. M., Oxholm, T. M., Siebert, G. L., Ade, P. A., Anderson, C. J., Barlis, A., Barrentine, E. M., Beeman, J., Bellis, N. G., Breyse, P. C., Bolatto, A. D., Bulcha, B. T., Cataldo, G., Connors, J. A., Cursey, P. W., Ehsan, N., Fernandez, L.-R., Glenn, J., Golec, J. E., Hays-Wehle, J., Hess, L., Jahromi, A. E., Kimball, M. O., Kogut, A., Lowe, L. N., Mauskopf, P., McMahon, J., Mirzaei, M., Moseley, H., Mugge-Durum, J., Noroozian, O., Pen, U.-L., Pullen, A. R., Rodriguez, S., Shire, K., Sinclair, A., Somerville, R. S., Stevenson, T. R., Switzer, E. R., Timbie, P., Tucker, C., Visbal, E., Volpert, C. G., Wollack, E. J., and Yang, S., “Optical design of the experiment for cryogenic large-aperture intensity mapping (EXCLAIM),” in [*Millimeter, Submillimeter, and Far-Infrared Detectors and Instrumentation for Astronomy X*], Zmuidzinas, J. and Gao, J.-R., eds., SPIE (dec 2020).
- [18] Wollack, E. J., Denis, K. L., Barlis, A., Chang, M.-P., Kuttyrev, A. S., Miller, K. H., and Nagler, P. C., “Far-infrared properties of cyclic olefin copolymer,” *Opt. Lett.* **45**, 780–783 (Feb 2020).